Elasticity and Poisson's ratio of hexagonal close-packed hydrogen at high pressures

Alexander F. Goncharov, Michel Gauthier, Daniele Antonangeli, Simon Ayrinhac, Frédéric Decremps, Marc Morand, Alexei Grechnev, S. M. Tretyak, and Yu. A. Freiman

Phys. Rev. B **95**, 214104 — Published 5 June 2017

DOI: 10.1103/PhysRevB.95.214104

Elasticity and Poisson's ratio of hexagonal close-packed hydrogen at high pressures

Alexander F. Goncharov*
Geophysical Laboratory, Carnegie Institution of Washington, 5251 Broad Branch Road NW, Washington DC 20015, USA

Michel Gauthier,† Daniele Antonangeli, Simon Ayrinhac, Frédéric Decremps, and Marc Morand
Institut de Minéralogie de Physique des Matériaux et de Cosmochimie (IMPMC), Sorbonne Universités - UPMC Université Paris 06, CNRS UMR 7590, Muséum National d'Histoire Naturelle, IRD UMR 206, 4 Place Jussieu, F-75005 Paris, France

Alexei Grechnev, S. M. Tretyak, and Yu. A. Freiman
B. Verkin Institute for Low Temperature Physics and Engineering, National Academy of Sciences, Prospekt Nauky 47, 61103 Kharkiv, Ukraine
(Dated: May 17, 2017)

The elasticity at high pressure of solid hydrogen in hexagonal close-packed (hcp) phase I has been examined experimentally by laser acoustics technique in a diamond anvil cell, up to 55 GPa at 296 K, and theoretically using pair and three-body semi-empirical potentials, up to 160 GPa. In the experiments on H_2 and D_2, the compressional sound velocity has been measured; the Poisson's ratio has been determined by combining these data with the previously reported equation of state. At room temperature, the difference between adiabatic and isothermal process vanishes above 25 GPa but can not be neglected at lower pressure. Theoretically, all five elastic constants of hcp hydrogen have been calculated, and various derived elastic quantities are presented. The elastic anisotropy of hcp hydrogen was found to be significant, with $\Delta P \approx 1.2$, $\Delta S_1 \approx 1.7$, and $\Delta S_2 \approx 1$. Calculations suggest the Poisson's ratio to decrease with pressure reaching a minimum value of 0.28 at 145 GPa. In the experiment, the Poisson's ratio is also found to decrease with pressure. Theoretical calculations show that the inclusion of zero-point vibrations (ZPV) on the elastic properties of H_2 does not result in any drastic changes of the behavior of the elastic quantities.

PACS numbers: 67.80.F-, 62.20.de, 62.20.dj
Keywords: solid hydrogen, elastic moduli, Poisson's ratio

I. INTRODUCTION

Solid hydrogen[1–3] has a rich phase diagram at high pressures (P), where a number of solid phases have been discovered. Below 200 GPa there are three major phases I, II, and III that correspond to a plastic (rotationally disordered) phase I and two orientationally ordered phases II and III[4,5]. Phases I and II show clear quantum properties related to the molecular rotational states[2,6], while phase III is suggested to be oriented in a classic sense[7,8]. Recently a number of new phases (IV to VI) have been discovered at pressures above 200 GPa[9–13]; these phases have been inferred to possess some features of atomic chemical structure. Interestingly, phase IV was proposed to have quantum properties related to the proton tunneling and pair fluctuations[14] and even unique mass-induced localization effects for the H_2-D_2 mixtures[15]. Due to highly diverse structural properties of H_2 solid phases, it is hard to follow the trend in the quantum properties with compression. This is magnified by the lack of direct structural information, which is essentially limited to phase I (see Ref.[16] for the latest on the subject and the available literature).

Quantum phenomena play important role for phase diagrams and various properties of low-Z materials, such as hydrogen. Solid hydrogen is the only molecular diatomic crystal which shows macroscopic quantum phenomena. However, at high pressures the balance between large zero-point vibrations (ZPV) and static lattice energy can be modified[17]. It is a surprisingly non-trivial question whether quantum effects become stronger or weaker as the pressure increases. Quantum effects in molecular systems were proposed to play an increasingly important role in the limit of very high densities resulting in melting in the $T = 0$ K limit[18,19] or even a transition to a superconducting superfluid state[20]. Other works argue that quantum effects become less substantial at high pressure[21,22] as the steeper interatomic potentials become a dominating factors over short-range correlations. However, one should point out that this discrepancy can be at least partially terminological. Under pressure, all energy scales are expected to increase as the interatomic potentials become steeper, including ZPV. Thus in order to understand the importance of quantum effects it is more informative to look at the relative strength of quantum effects, as done here by monitoring the pressure evolution of the Poisson's ratio (PR).

The strength of quantum effects can be estimated experimentally[23] by comparing results for H_2 and D_2 (the latter having twice the mass of the former and thus presenting a much less quantum behavior). Calculations offer the simpler option by comparing results with

and without ZPV included. In H_2 at low pressures, both translational and rotational excitations have strong quantum nature that is the consequence of the weak intermolecular interaction and light mass[2]. ZPV in hydrogen is anharmonic, thus strictly speaking quasi-harmonic (QH) lattice dynamics cannot be applied in this regime. In practice, however, QH approximation is often used as an approximate estimate of the translational ZPV. As the result of the strong translational ZPV, solid H_2 is highly compressible[23]. Also the molecular positions are highly spread out, thus the intermolecular interactions are sometimes renormalized to account for lowering of phonon frequencies[2].

Phase I (hcp) of solid hydrogen is stable up to 100-250 GPa, depending on the temperature[4,5,12]. It consists of nearly freely rotating molecules, and this motion is quantized ($J = 0, 1, 2, \ldots$) resulting in a number of rotational energy levels that can be probed through the observations of transitions between them. The molecules are spherically symmetric in the $J = 0$ ground state. At higher pressures hydrogen I undergoes phase transitions to orientationally ordered (II, III) and partially atomized (IV-VI) phases. The presence of quantum effects in hydrogen at very high pressures has been recently shown experimentally: quantum tunneling effects and phonon localization were found in phase IV above 250 GPa[10,14,15].

High-pressure elastic properties of solid hydrogen give insight into anisotropy, equation of state, thermodynamic properties, and intermolecular potentials of this material. Potentially, they can also provide an important link to structural phase transitions in H_2 and ultrahigh pressure behavior approaching transformation to metallic or atomic phases. The Poisson's ratio (PR)[24] defined as a ratio of the negative lateral to the axial strain for an axially strained sample has been recognized as one of fundamental thermodynamic properties of an isotropic elastic medium, and a polycrystalline solid is usually a good approximation to the isotropic one. The PR (σ) is uniquely determined by the ratio of the bulk modulus K to the shear modulus G

$$\sigma = \frac{3K/G - 2}{2(3K/G + 1)} \tag{1}$$

In principle, it can vary from -1 to 0.5 since the K/G ratio may vary from 0 to infinity. However, a more detailed analysis shows that PR normally lies between 0.2 and 0.5 unless the samples are very hard or porous[25]. In fact, a typical PR value for metals is about 0.3. Under pressure, PR increases if the increase with pressure of the shear modulus is slower than that of the bulk modulus, and decreases in the opposite case. It has been also shown[26] that $d\sigma/dP$ is related to the pressure dependence of the Grüneisen parameter and other thermodynamic quantities. Thus, the pressure dependence of the PR can be used as a sensitive test of materials behavior including interatomic interactions and, through this, of quantum effects. Due to the way the PR is constructed, it can be used to evaluate the effect of the relative strength of the quantum effects as we do below by calculating its values with and without ZPV included.

In the pressure range of tens of GPa the problem has been investigated by Brillouin scattering for a number of materials[27–29]. The $\sigma(P)$ dependence is usually monotonous. It has been speculated[27] that most materials reach the asymptotic value close to 0.3 (characteristic for metals) at very high pressures, thus σ is commonly expected to increase with pressure if $\sigma(0) < 0.3$, and decreases with pressure in the opposite case. From a theoretical point of view, it has been demonstrated[30] that PR decreases monotonously for hcp helium in agreement with the experiment[28], reaching the value of 0.29 at 30 TPa. For hcp hydrogen in phase I it has been estimated[31], based on the behavior of the elastic constant C_{44}, that σ also decreases with pressure but no calculation of all five independent elastic constants C_{ij} has been performed until now.

The stiffness tensor C_{ij} of solid hexagonal close-packed (hcp) H_2 has been determined experimentally up to 24 GPa from single-crystal sound velocities measured with the Brillouin scattering technique[29,32,33]. Also, the elastic anisotropy, Cauchy violations, and aggregate elastic properties (within the Voigt-Reuss-Hill averaging scheme) such as the sound velocities, the bulk and shear moduli, and the Poisson's ratio have been derived[29].

The goal of the present paper is to examine the elasticity and the Poisson's ratio of hcp hydrogen phase I at pressures higher than the 24 GPa of Ref.[29] to determine the trend in the highly compressed states. However, Brillouin spectroscopy measurements at pressures above 24 GPa are challenging because of the reduced sample volume and the necessity to have a large angular optical access. In the present work, we report compressional sound velocity measurements up to 55 GPa by picosecond laser acoustics (PLA) technique[34–36], which has much less strict limitations for the scattering volume and optical access. We have combined the direct measurements of the compressional sound velocities of this work with the equation of state determined previously[25], to determine the transverse sound velocities and the Poisson's ratio up to 55 GPa. On the theoretical side, we calculated the five elastic constants C_{ij} of H_2-I up to 160 GPa using 2- and 3-body semi-empirical (SE) potentials, and employing the procedure we used previously for helium[30]. Knowledge of C_{ij} allows us to obtain a number of elastic quantities, including the PR, which we compare to the Brillouin scattering data[29] and to our PLA data where applicable.

II. METHODS

A. Experiment

Hydrogen and deuterium were loaded in a diamond anvil cell (DAC) with flat 300 μm culets together with Al transducers which convert laser radiation to sound waves

(Fig. 1). This configuration is necessary for transparent samples, but not for experiments with opaque samples, where sample itself serves as a transducer[34–36]. A rhenium gasket was precompressed to 40 μm thickness, and a round hole of 180 μm in diameter was drilled in the middle of the indentation using a sub-ns laser drilling machine. The diamond culets were partially coated by thin ($\approx$ 0.2 μm) Al layers formed by compressing small Al particles between two anvils with parallel culets. The thickness of the Al coatings was estimated to be close to 210 nm at 2.5 GPa using the observations of interference fringes which occur in spectrally analyzed reflected white light beam probing the area adjacent to the deformed aluminum particle. To reduce the scattering of the probing laser beams, we avoid using ruby for pressure measurements. Pressure in the cavity was determined using the spectral position $\nu(P)$ of the H_2 (or D_2) molecular vibron band measured before and after each PLA measurement. These measurements were also complemented by the Raman measurements of the stressed diamond anvils. In the pressure range near the maximum of the $\nu(P)$ curves of H_2 (or D_2), pressure was determined using the extrapolated linearly stressed diamond pressure. The pressure accuracy was estimated to be $\pm$0.25 GPa using this approach. H_2 and D_2 of research purity were gas-loaded in a high-pressure vessel at approximately 0.17 GPa. All experimental measurements have been performed at T=297 K. Thus, we refer our measurements to mixed ortho-para hydrogen (n-H_2 or n-D_2).

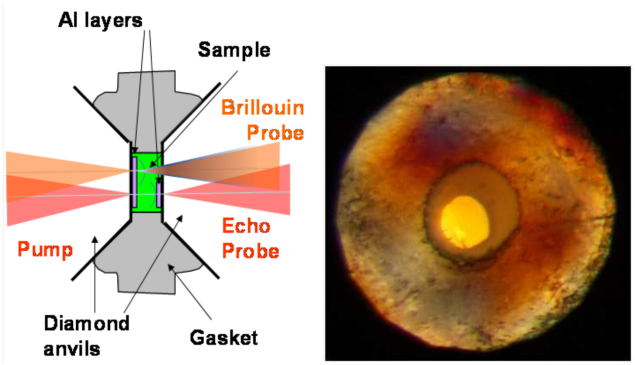

FIG. 1. Experimental details: (a) The experimental schematic of picosecond laser acoustic measurements in a DAC. The pump and the probe beams are introduced through the opposite diamond anvils. The pump beam is focused into a transducer made of a 0.2 μm thick Al layer that partially coats a culet of one anvil. A second but smaller Al layer (optional) which is deposited on the second diamond culet serves as a transducer for the echo probe from acoustic wave traversing the cavity, while the Brillouin probe records the spatially resolved sound wave propagating through the cavity. (b) A microphotograph of a sample at 1 GPa after high-pressure H_2 gas loading.

An picosecond laser acoustic setup for measurements of sound velocities at high pressures at IMPMC has been previously described[34]. An extensive experimental and theoretical review of the capabilities of the PLA has been published in a dedicated volume of Ultrasonics[37]. In brief, a λ=800 nm wavelength pulse train of about 100 fs delivered by a Ti-Sapphire femtosecond oscillator with 80 MHz repetition rate, is split into pump and probe beams. The pump beam, which is modulated by an acousto-optic modulator at a 1 MHz, periodically heats and locally expands an internal Al transducer creating a compressional acoustic wave propagating across the sample (Figs. 1- 2). The probe beam passes a controllable mechanical scanning optical delay line and is split by a stabilized Michelson interferometric system[38] into two channels in one of which the beam is focused to the sample area from the opposite side of the DAC. A lock-in amplifier synchronized with the modulation frequency is used to improve the signal-to-noise ratio.

Two techniques were used to extract the compressional sound velocities of the sample. In the Brillouin configuration (which is different of a conventional Brillouin spectroscopy where the experiments is performed in a frequency domain), the probe beam is focused in the transducer which is directly pumped and the reflected light is modulated by interference between the probe beam and the propagating acoustic wave fronts (Fig. 2(a)) recorded in the time domain. The sound velocity c is extracted from the relation $f = 2nc/\lambda$, where f is the frequency of oscillations, n is the refractive index and λ is the laser wavelength. In principle, the increased bandwidth of the laser contributes to the uncertainty in the frequency determination. However, the oscillations in the time domain are quite well modulated making the frequency extraction quite certain thereby allowing to record the spatial variations (Fig. 3). In the echo configuration, the probe beam is focused on the surface of the second transducer and the reflected beam records an anomaly (bump or dip) corresponding to the time of arrival of the acoustic wave passing the whole cavity (Fig. 2(b)). As the second transducer does not cover the entire diamond surface, collection of both the Brillouin signal from the H_2 sample and the echoes is expected as it can be seen on the figure 2(b).

The probe beam reflected from the primary transducer is modulated by an acoustic wave for a period of time of about 1 ns (up to 4 ns in liquid) after the arrival of the pump beam (Fig. 2(a)). This corresponds to a distance of approximately 10 μm across the sample, where the different parts of the sample can be effectively probed locally. In the liquid state, we naturally observe that the Brillouin frequency is spatially uniform (Figs. 3(a,c)). However, in the solid state the compressional sound velocity varies from point to point across the sample with a typical characteristic length of > 0.3 μm, which should be understood as due to a directional dependence of the compression sound velocity in the moderately elastically anisotropic solid hcp-H_2[29] (Figs. 3(b,d)). The ability of PLA to measure sound velocity variations in spatially inhomogeneous sample (see also Ref.[39]) suggests that the

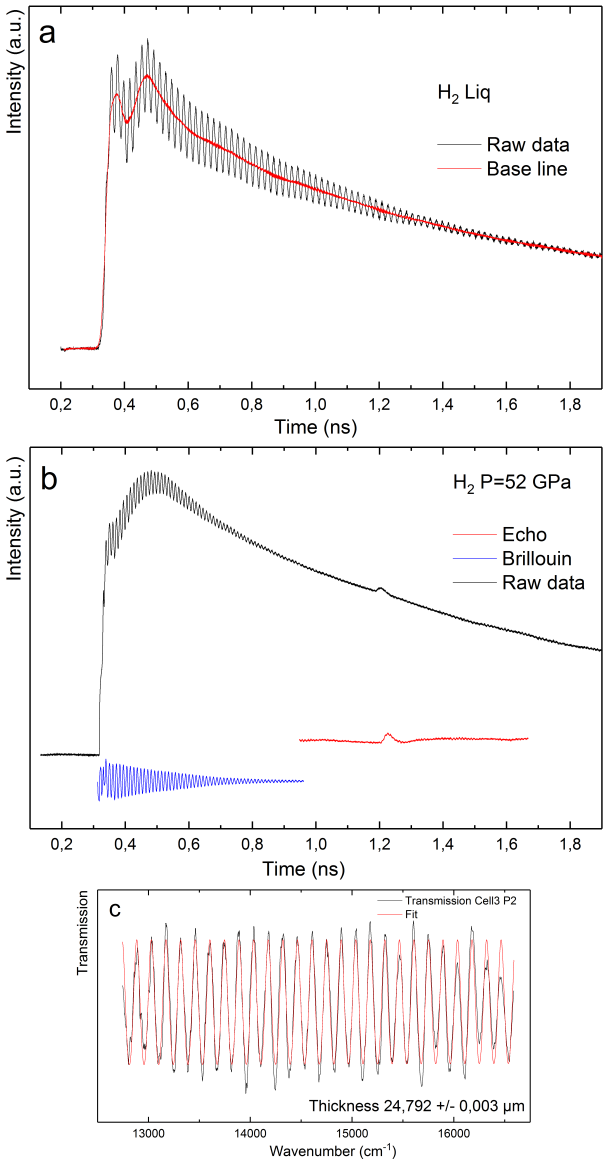

FIG. 2. Experimental observables : (a) The reflectivity signal (raw data) of the Al transducer measured as a function of time delay showing the Brillouin modulation superposed on the expected base line (smoothened line in red) in absence of Brillouin signal; (b) An example of the echo observation (red curve) which corresponds to the time of arrival of the acoustic wave propagated across the sample. Also plotted (in the same time-scale) is the raw signal of the first transducer including echo (acoustic wave reflected from the second transducer back to the first one) and Brillouin signal (extracted blue curve); (c) White light transmission spectrum (normalized) through the DAC cavity which shows Fabry-Perot interference fringes due to multiple reflections of the diamond-sample interfaces.

acoustic anisotropy can be evaluated by probing crystallites with various crystallographic orientations thus making it possible to assess the stiffness tensor; this is beyond the scope of this work. Nevertheless these assumptions have been tested at 25.3 GPa on a grained H_2 sample, and all the measured longitudinal sound velocities are in a 16-17 km/s range in very good agreement with expected values (16-16.9 km/s) derived from the C_{ij} quantities at 23.6 GPa reported by Zha *et al.*[29].

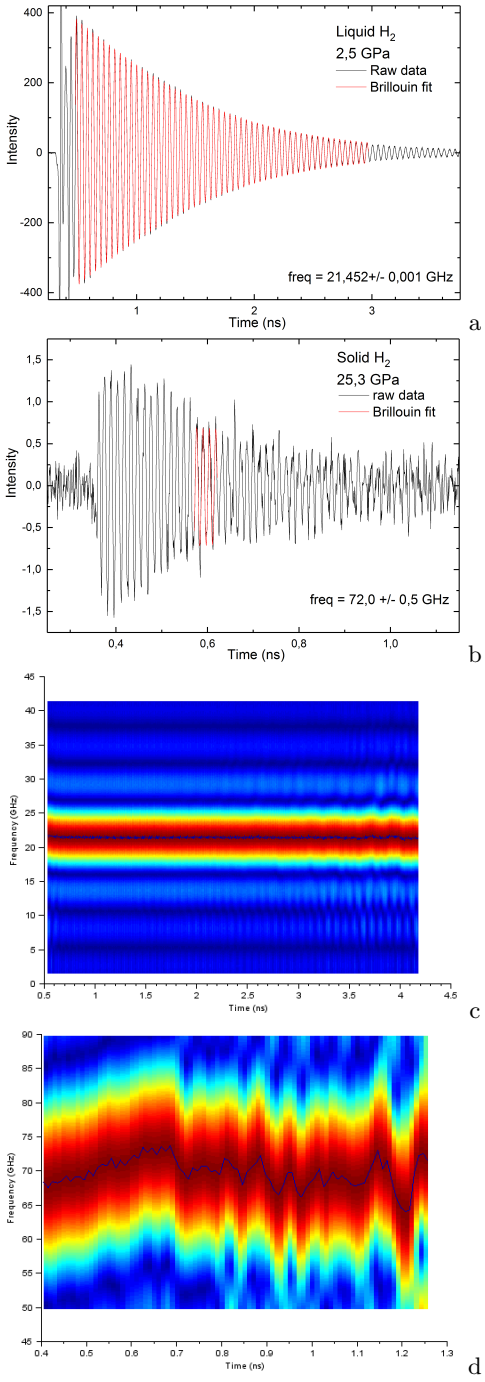

FIG. 3. Brillouin sound velocity determination in H_2 in liquid (a,c) and solid (b,d) states. (a,b) Time series of the reflectivity for liquid (2.5 GPa) and solid (25.3 GPa); (c,d) Brillouin frequencies determined from fitting of the data in (a,b) as a function of time delay corresponding to spatial probing of H_2 sample along the DAC axis.

Both the techniques used here to determine the com-

pressional sound velocity (time-resolved Brillouin and pulse-echo techniques) require the knowledge of the refractive index n of H_2. We have used the results of Refs.[40,41] for the wavelength dependent n in liquid H_2 and for the pressure dependent n of H_2 in liquid and solid phases, respectively. We assumed that the refractive index of D_2 is identical following the results of Brillouin measurements of Shimizu *et al.*[33]. The wavelength dispersion of n in Ref.[40] can be conveniently expressed as

$$n(\lambda) = \left[1 + \frac{F(P)}{1 - (E(P)/\lambda)^2}\right]^{1/2} \quad (2)$$

where $F(P)$ and $E(P)$ are the pressure dependent oscillator strength and energy, respectively, related to the effective oscillator corresponding to the electronic valence band transition. We used the literature data for the pressure dependent electronic oscillators to determine the dispersion correction of n from $\lambda = 632.8$ nm (used in Ref.[41]) to 800 nm. To determine the DAC cavity thickness at each P point, we have measured white light interference fringes in transmission spectra between 550 to 800 nm (Fig. 2(c)). The DAC cavity thickness was determined by fitting it by the standard Fabry-Perot interferometry formalism using the refractive index expressed by Eq. 2. To determine the sample path length we have corrected for the two Al transducer thicknesses, which were determined using the observations of echo in the Al foils for each pressure points (from 32.5 ps at 2.6 GPa to 18 ps at 55 GPa) and the known compressional sound velocity of Al, yielding a small decrease of the transducers thicknesses from about 210 nm at room pressure to 180 nm at the highest pressure reached in the experiment. Small disagreements between the time-resolved Brillouin and pulse-echo techniques could be due to non-perfect contact between diamond tips and Al foil determined to be within 500 nm, which is consistent with the optical observations. This effect results in overestimation of the distance between the Al foils and hence of the sound velocity. On the other hand, the effect of diamond cupping which was not taken into account here would tend to underestimate this distance as the diamond-diamond distance was measured closer to periphery where it is smaller. In the case of D_2 experiment the results obtained with the echo technique disagree substantially because the second transducer peeled off once the sample solidified; these results were not included in the reported data set.

The measured compressional sound velocity in combination with the EOS from Ref.[23] can be used to find the shear sound velocity and the Poisson's ratio. Equation 1 can be easily transformed to

$$\sigma = \frac{3K_S - M}{3K_S + M} \quad (3)$$

where K_S is the adiabatic bulk modulus and $M = \rho c_P^2$, where c_P is the compressional sound velocity and ρ the density. Note that the isothermal bulk modulus K_T deduced from the EOS needs to be transformed to adiabatic one by the following relation $K_S = K_T + \rho C_V \Gamma^2 T$, where C_V is the specific heat at constant volume, Γ the Grüneisen parameter, and T the temperature. This correction corresponds to the Laplace coefficient γ_L

$$\gamma_L = C_P/C_V = K_S/K_T = \left(1 + \rho C_V \Gamma^2 T/K_T\right) \quad (4)$$

(C_P the specific heat at constant pressure) which has been shown to be strongly pressure dependent; the correction decreases from 13% to 1.5% between 6 and 24 GPa[29].

B. Theory

We have calculated the five elastic constants C_{ij} (defined as stress-strain coefficients) of hcp phase I of H_2 at variable pressures using semi-empirical pair and three-body potentials as presented in details in Refs.[30] and[42]. The elastic constants were found from the equation of state and three independent isochoric strains : uniaxial (varying c/a ratio), orthorhombic, and monoclinic. The aggregate properties (sound velocities, Poisson's ratio) were then calculated from the C_{ij}s using Voigt-Reuss-Hill averaging scheme. Zero-point vibrations were introduced within the quasi-harmonic Debye approximation for hydrogen. All our calculations have been done at T=0 K. The long-distance cutoffs of 50.2 and 10.2 lattice constants have been used for pair and triple forces respectively. A few issues must be clarified here. First, unlike helium[30], hydrogen has rotational degrees of freedom. In our present calculations we ignore rotations and treat H_2 molecules as spherically symmetric. This is a reasonable approximation for the low pressure phase I, where H_2 molecules are quantum rotors in the $J = 0$ ground state to a good extent. Second, our quasi-harmonic treatment of the zero-point vibrations of molecules is rather crude. As discussed above, ZPV of hydrogen molecules is anharmonic, at least at low pressures. However, the calculation of elastic constants requires a high numerical accuracy and a large number of total-energy calculations, including ones for deformed (non-hcp) lattices. This is why we decided to start with a simpler approach which nevertheless allows us to estimate the magnitude of the quantum effects. Third, we used exactly the parametrization of pair and three-body forces as previously done in Refs.[31,43–46]. Specifically, the pair potential (energy of a pair of H_2 molecules) is

$$U_2(R) = exp(\alpha - \beta R - \gamma R^2) - f_C(R) \sum_{n=6,8,10} C_n R^{-n}$$

$$f_C(R) = \begin{cases} exp[-(R^*/R - 1)^2] & , R < R^* \\ 1 & , R > R^* \end{cases}$$

R being the distance between two molecules and $R^* \equiv DR_m$. The pair potential parameters are $\alpha = 1.713, \beta = 1.5671, \gamma = 0.00993, C_6 = 12.14, C_8 = 215.2, C_{10} =$

4813.9, $D = 1.28$, $R_m = 6.44$, all in Hartree atomic units. The three-body potential (energy of a triangle) is

$$U_3(r_1, r_2, r_3) = (1 + 3\cos\Phi_1 \cos\Phi_2 \cos\Phi_3) \times$$
$$-A\ exp\left\{-B(r_1 + r_2 + r_3) + C\frac{\sqrt{f_C(r_1)f_C(r_2)f_C(r_3)}}{r_1^2 r_2^2 r_3^2}\right\}$$

where $A = 6.085$, $B = 0.737858$, $C = 49.49815$, r_1, r_2, r_3 are the three sides of the triangle and ϕ_1,ϕ_2,ϕ_3 are the three angles between the sides. The total energy of the crystal is

$$E = \frac{1}{2}\sum_{R_1 \neq R_2} U_2(|R_1 - R_2|)$$
$$+\frac{1}{3!}\sum_{R_1 \neq R_2 \neq R_3} U_3(R_1 - R_2, R_2 - R_3, R_3 - R_1)$$

where R_i are the crystal lattice sites.

III. RESULTS

A. Elastic constants, anisotropy, Cauchy violations

The five elastic constants (independent components of the stiffness tensor C_{ijkl}) of hcp hydrogen obtained with semi-empirical potentials are presented in Fig. 4 versus pressure up to 160 GPa. The results obtained without zero-point vibrations (ZPV) are also shown. We compare our computational data to the Brillouin spectroscopy data of Zha *et al.*[29] (up to 24 GPa), the only available experimental data on the elastic moduli of H_2 in the GPa pressure range. There is a reasonable agreement between our data and the experiment. Also, note that the experiment[29] has been performed at room temperature, while our calculations were done for T=0 K.

The hcp structural stability conditions[47,48] $C_{44} > 0$, $C_{11} > |C_{12}|$ and $C_{33}(C_{11} + C_{12}) > 2(C_{13})^2$ are fulfilled, which means that hcp hydrogen is mechanically stable over the whole considered pressure range. Note, a somewhat nonlinear behavior of C_{13} with pressure and the crossing of C_{13} and C_{44} pressure curves at about 70 GPa (Fig. 4). No experimental data on C_{ij} exist for this pressure range at present, so we cannot test this prediction obtained with 2- and 3- body SE potentials. From the comparison of solid (with ZPV) and dotted (without ZPV) curves in Fig. 4 one can see that within our quasi-harmonic Debye approximation the quantum effects, while noticeable, do not alter the behavior of $C_{ij}(P)$ in any drastic way, at least for pressures up to 160 GPa. Figure 5 presents the three elastic anisotropy parameters of hcp hydrogen

$$\Delta P = \frac{C_{33}}{C_{11}},$$
$$\Delta S_1 = \frac{C_{11} + C_{33} - 2C_{13}}{4C_{44}},$$
$$\Delta S_2 = \frac{2C_{44}}{C_{11} - C_{12}} = \frac{C_{44}}{C_{66}}.$$

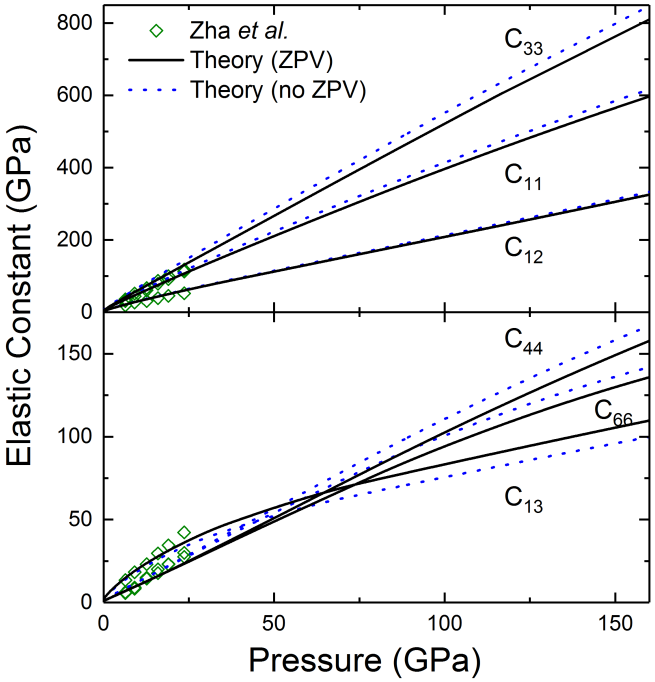

FIG. 4. The elastic constants of hcp H_2 versus pressure obtained with semi-empirical potentials with and without including zero-point vibrations (ZPV). Experimental data of Zha *et al.*[29] are also presented.

These parameters characterize the anisotropy of the three major acoustic modes, which in turn indicate the anisotropy of the stiffness tensor C_{ijkl}. For an isotropic solid $\Delta P = \Delta S_1 = \Delta S_2 = 1$. Note that the physical quantities represented by a second rank tensor (such as conductivity, dielectric permittivity, etc.) are exactly isotropic for cubic crystals and approximately isotropic for hcp crystals. This is not the case for tensors of rank 4 such as C_{ijkl}. Indeed, for most crystals, including cubic and hcp ones, the stiffness tensor C_{ijkl} is far from isotropic. One can see from Fig. 5 that ΔS_2 is close to 1, while $\Delta S_1 \approx 1.7$ and $\Delta P \approx 1.2$. The theory provides a correct order of magnitude of these three parameters compared to the experiment of Zha *et al.*[29], only slightly overestimating the anisotropy for ΔS_1. Again, there could be a difference between T=0 K (theory) and room temperature (experiment) values, which can explain a small disagreement. However, one can see that the pressure dependencies of ΔP, ΔS_1, ΔS_2 disagree substantially but we will see later in this paper (Fig. 11 and Sec. III C) that the low pressure experimental results are biased by an underestimation of the adiabatic to isothermal correction. Finally, the effect of ZPV on the elastic anisotropy is small and the largest contribution is found for ΔP. The Cauchy violations $3C_{12} - C_{11} - 4P$ and $C_{13} - C_{44} - 2P$, where P is the hydrostatic pressure, are presented in Fig. 6. In this case, there is a

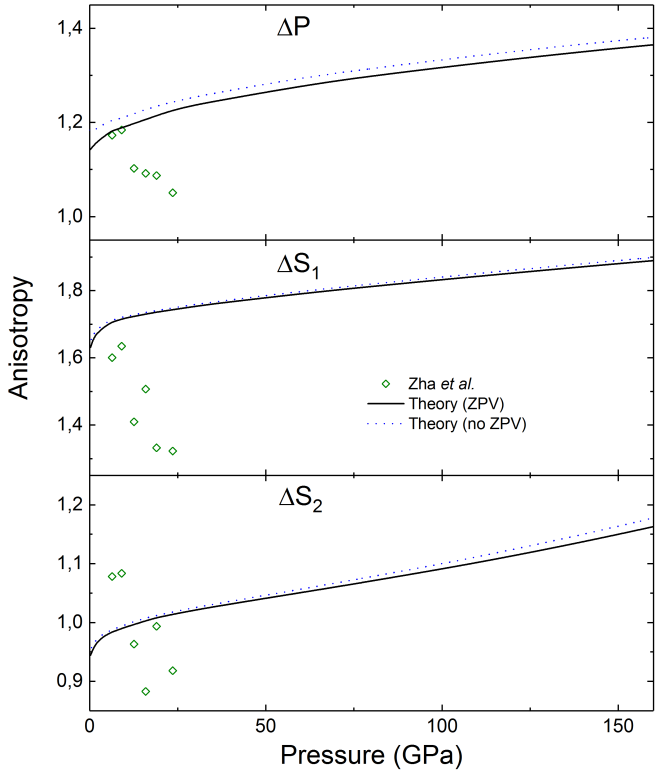

FIG. 5. The elastic anisotropy parameters of hcp H_2 versus pressure.

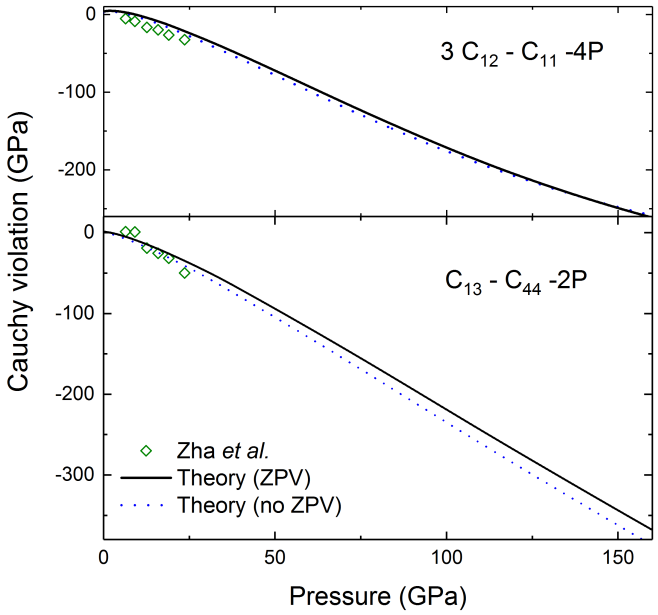

FIG. 6. Cauchy violations of hcp H_2 versus pressure.

reasonably good agreement between our theory and the experiment. Note that the effect of ZPV is significant for $C_{13} - C_{44} - 2P$, but not for $3C_{12} - C_{11} - 4P$.

B. Aggregate sound velocities, bulk and shear moduli

Aggregate physical quantities are defined for an isotropic (or polycrystalline) solid. They include bulk and shear moduli K and G, the Poisson's ratio defined in Eqs.(1, 3) and the compressional (c_P) and shear (c_S) sound velocities

$$c_P = [(K + \frac{4}{3}G)/\rho]^{1/2}, c_S = (G/\rho)^{1/2}. \qquad (5)$$

The bulk sound velocity determined as $c_B = (K/\rho)^{1/2}$, corresponds to the compressional mode of the liquid phase. Among the three sound velocities only two are independent, since $c_B^2 = c_P^2 - 4c_S^2/3$. In theoretical treatment, they are linked to $\overline{C_{11}}$, $\overline{C_{12}}$ and $\overline{C_{44}}$ the elastic constants obtained from single crystal C_{ij} and the Voigt-Reuss-Hill averaging procedure with $c_P^2 = \overline{C_{11}}/\rho$, $c_S^2 = \overline{C_{44}}/\rho$ and $c_B^2 = \left(\overline{C_{11}} - 4\overline{C_{44}}/3\right)/\rho$.

Experimentally, aggregate quantities are found either from experiments on polycrystalline samples, or using some kind of averaging procedure of the single-crystal sound velocities. In our experiment, the average compressional velocities were found from the experimental Brillouin frequencies.

Our data at 25 GPa (Figs. 3(b, d)) show a span of values (c_{min}=16 km/s, c_{max}=17 km/s, $\delta c/c$=0.06) of compressional sound velocities determined from their spatial dispersion, which compares well with those (16 km/s-16.9 km/s, 0.06) determined in Ref.[29] from the angular dispersion of the compressional velocity at 23.6 GPa. On some runs the sample was found to be highly disordered with a good polycrystalline quality as shown in Fig 7. and give access directly to the mean values of the elastic constants $\overline{C_{11}}$, $\overline{C_{12}}$ and $\overline{C_{44}} = (\overline{C_{11}} - \overline{C_{12}})/2$ expected for an isotropic crystal.

The experimental compressional sound velocities of H_2 and D_2 as a function of pressure are presented in Fig. 8. For D_2 we have included the usual $\sqrt{2}$ scaling factor due to the difference in molecular masses. We can see that they differ by a few percent at most in the pressure range considered. This difference (with the $\sqrt{2}$ scaling factor included) is a measure of the quantum effects in hydrogen. The results show strong pressure dependence in a good general agreement with the previously reported data at smaller pressures[29,32,33]. Both in the liquid and solid phase, our data agrees well with the Brillouin results of Shimizu *et al.*[33]. Following Shimizu, in the solid phase, our data on the compressional sound velocity c_P are best approximated by the simple equation $c_P = aP^b$, where P is in GPa, a=6.02 km/s and b=0.311 (respectively 5.75 km/s and 1/3 in Ref.[33]).

The isotropic elastic constants $\overline{C_{11}}$, $\overline{C_{12}}$ and $\overline{C_{44}}$ deduced from these results and a hypothesis of the perfect polycrystal are shown in Fig. 9. The longitudinal and

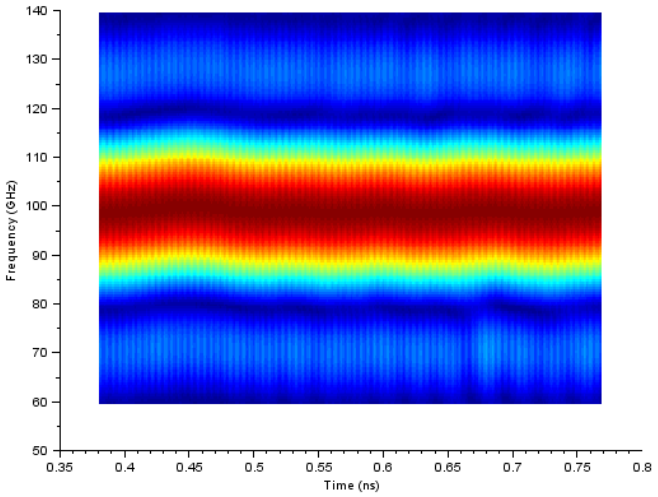

FIG. 7. Brillouin frequency distribution in H_2 at 55 GPa. The Brillouin frequencies are determined from fitting of the data as a function of time delay corresponding to spatial probing of H_2 sample along the DAC axis. In contrast to Fig. 3(b,d), the sample exhibits very high polycrystallinity and Brillouin frequency is almost constant over the whole sample volume.

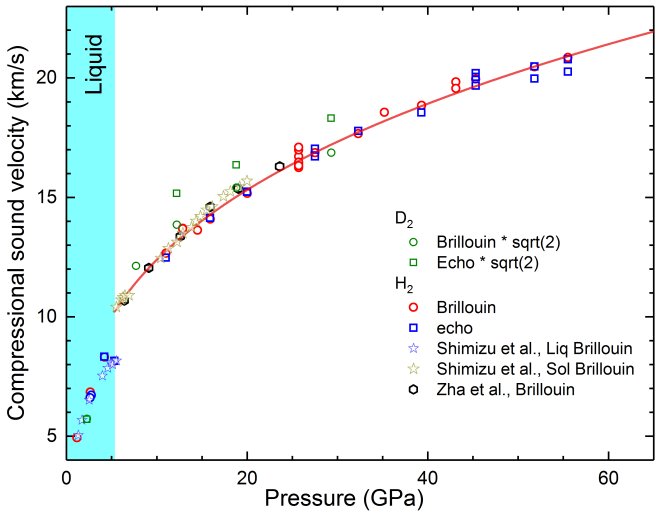

FIG. 8. Compressional sound velocity of H_2 and D_2 at high pressure measured in this work using PLA in comparison to the previous results obtained using a conventional Brillouin spectroscopy[29,33]. The sound velocities of D_2 are multiplied by $\sqrt{2}$. The solid line corresponds to the best fit of expression $c_P(P) = aP^b$ with a=6.02 km/s and b=0.311 .

transverse velocities reported by Shimizu *et al.*[33] have been combined with the EOS reported by Loubeyre *et al.*[23]. The results of Zha plotted here have been obtained using the Voigt-Reuss-Hill averaging procedure. There is a good agreement between our results, previous experimental data and our theoretical values except for the $\overline{C_{12}}$ values deduced from Shimizu's data.

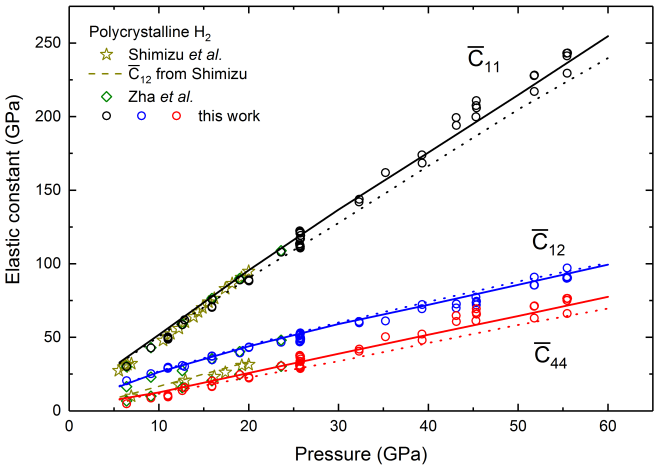

FIG. 9. H_2 isotropic elastic constants derived within the perfect polycrystal approximation. The solid lines are our theoretical results with ZPV (solid lines) and without ZPV (dashed lines). The results referred to Zha *et al.* have been obtained from ref.[29] using the classical Voigt-Reuss-Hill averaging procedure. To extract C_{ij} from Shimizu *et al.*[33] we combined their raw data and the EOS published in Ref.[23].

The theoretical velocities c_P, c_S and c_B are presented in Fig. 10 in a wider pressure range (up to 160 GPa). There is a good agreement with the experiment[29]. It should be noticed that the effect of ZPV (quantum contribution) on the sound velocities is small in our calculations in the whole pressure range. Without any surprise, our calculation of theoretical aggregate bulk (K), shear (G) moduli of hcp H_2, which are directly related to c_B and c_S, compared favorably to the experimental data.

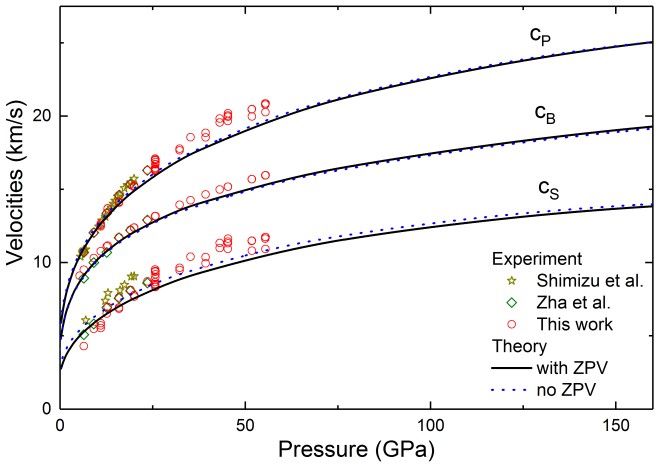

FIG. 10. Compressional, bulk and shear sound velocities of hcp H_2 in the 160 GPa pressure range. Theoretical (this work) and experimental (this work and Refs.[29,33]) results are presented.

The Debye temperature (T_D) of hcp H_2 can be easily

extracted from the mean sound velocities c_P and c_S

$$T_D = \frac{\hbar}{k_B}\left[\frac{V_{mol}}{18\pi^2 N_A}\left(\frac{1}{c_P^3}+\frac{2}{c_S^3}\right)\right]^{-1/3} \quad (6)$$

and used to calculate the specific heat at constant volume C_V since

$$C_V = 9N_A k_B\left(\frac{T}{T_D}\right)^3\int_0^{T_D/T}\frac{x^4 e^x}{(e^x-1)^2}dx \quad (7)$$

At room temperature and for pressure lower then 25 GPa, the integral part is far from $4\pi^4/15$ and has to be calculated since the $T \ll T_D$ condition is not fulfilled (see Fig. 11). Finally, the determination of the Grüneisen parameter Γ

$$\Gamma = \frac{1}{3}+\frac{\partial \ln \bar{c}}{\partial \rho} \quad (8)$$

where $\bar{c}$ is the mean velocity, allows the calculation of the Laplace coefficient γ_L (see Eq. 4). The main results are shown in Fig. 11. Clearly, all results are in good agreement except for the low pressure experimental Laplace coefficient values determined from the experimental C_{ij} from Zha *et al.*[29]. At room temperature, above 25 GPa, the difference between adiabatic and isothermal bulk modulus vanished since the Laplace coefficient $\gamma_L \approx 1$.

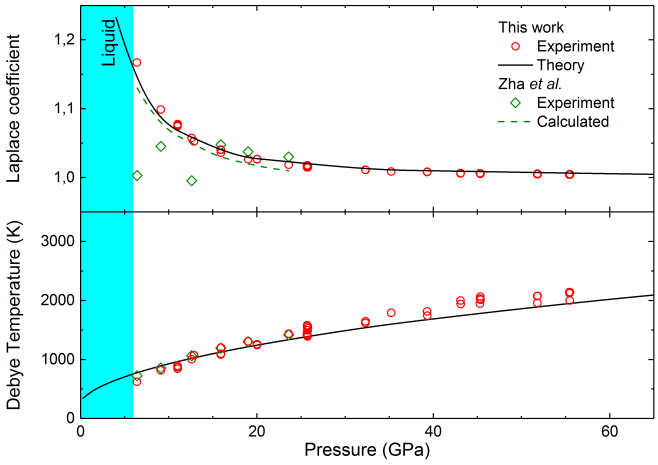

FIG. 11. Theoretical and experimental results for the Debye temperature and the Laplace coefficient of hcp H_2.

C. Poisson's ratio

The Poisson's ratio as a function of pressure obtained from our experimental data and the EOS of Ref.[23] through Eq. 3 is shown in Fig. 12. Our data on PR below 24 GPa are expected to be in agreement with the results of Zha *et al.*[29] as the compressional sound velocities agree and also the equations of state which have been used here and in Ref.[29] are very similar[23,49]. The values proposed by Zha correspond to our raw data without the isothermal to adiabatic correction of the bulk modulus used to extract the PR values. This is due to the use of the non adiabatic equation (7) in the Zha *et al.* paper[29] to obtain an essential relation between elastic constants. Nevertheless, as the pressure increases this correction decreases and becomes negligible at high pressure (less than 1% above 30 GPa). As for the helium case[28,30], the calculated PR of hydrogen decreases with pressure, supporting the idea[27] of PR approaching an asymptotic value close to 0.3 as pressure increases. Our experimental data, while showing some scattering, qualitatively agree with this prediction (Fig. 12). However, higher pressure data are needed to accurately establish the asymptotic behavior. Our theoretical results in the 160 GPa pressure range are presented in Fig. 13. Our theory finds a shallow minimum at about 145 GPa (or 120 GPa if ZPV are not included), where PR is approximately 0.28, which is slightly less than the value 0.3 suggested in Ref.[27], and close to the PR in helium at terapascal pressures[30].

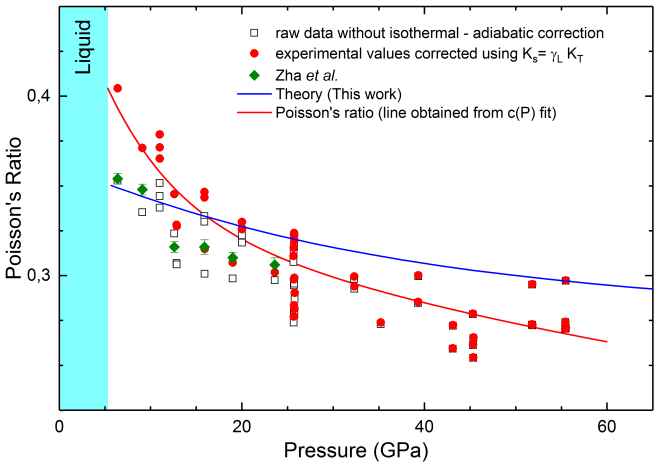

FIG. 12. The Poisson's ratio of H_2 deduced using Eq. 3 from our measurements of the compressional sound velocity and the EOS of Ref.[23]

A pseudo-Poisson's ratio, which uses C_{44} instead of G,

$$\sigma' = \frac{3K/C_{44}-2}{2(3K/C_{44}+1)}, \quad (9)$$

is also presented in Fig. 13. This quantity has been used previously[31] to estimate the pressure dependence of σ. The behavior of σ' is qualitatively similar to that of σ, but quantitatively they are rather different.

Let us now return to the question of the importance of quantum effects, and how their magnitude changes with pressure. By comparing the behavior of PR calculated with and without ZPV (Fig. 13), one can see that the ZPV contribution to the PR value is rather substantial, larger than for the majority of quantities described above, but it does not change its pressure dependence in any fundamental way. We therefore speculate that the pressure

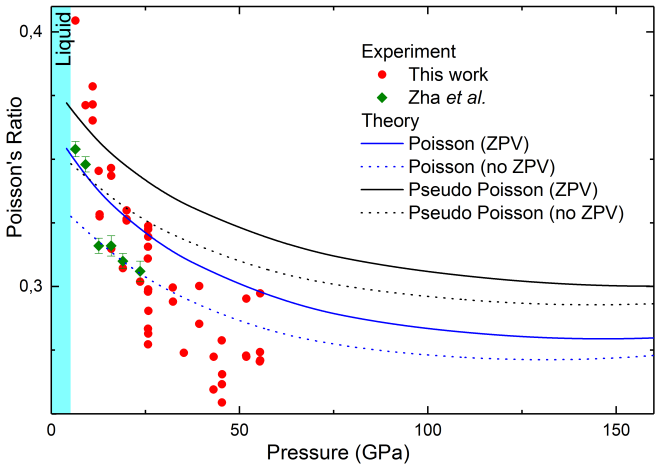

FIG. 13. Theoretical and Pseudo Poisson's ratio of H_2 in the 160 GPa pressure range compared to experimental data.

dependence of PR is classical in nature with significant quantum corrections originating from translational degrees of freedom (rotational and vibrational degrees of freedom are considered as inherently quantum in phase I of H_2). The relative ZPV contribution to PR and other quantities presented above decreases slowly with pressure in the 5-160 GPa pressure range. Our previous work on helium[30] showed similar behavior in the same pressure range, and the ZPV contribution decreased even more noticeably in the terapascal range.

IV. CONCLUSION

We have measured the compressional sound velocity in hcp hydrogen phase I up to 55 GPa at T=297 K using the picosecond laser acoustics technique. By combining these results with the previously reported equation of state[23] we determined the Poisson's ratio versus pressure. The Poisson's ratio decreases with pressure with a possible minimum at about 50 GPa.

We have also calculated the five independent elastic constants C_{ij} of hcp H_2 up to 160 GPa at T=0 K using semi-empirical pair and three-body potentials. Pressure dependencies of various elastic quantities derived from C_{ij} are examined : elastic anisotropies, Cauchy violations, bulk and shear moduli, aggregate sound velocities, Debye temperature, Laplace coefficient and the Poisson's ratio. There is a generally good agreement with the available experimental data except for some previously reported results at low pressure. We point out that at room temperature, the difference between adiabatic and isothermal process vanishes only above 25 GPa but can not be neglected at lower pressure which can contribute to the mentioned above discrepancy. The theoretical Poisson's ratio shows a decrease with increasing pressure and reaches a shallow minimum at 145 GPa and σ = 0.28. The quantum effects (introduced as translational ZPV) are significant for the PR values but do not change qualitatively the $\sigma(P)$ dependence. The quantum effects affect less other examined elastic quantities. Overall, the quantum contribution to the elastic quantities is found to be marginal and to decrease slowly with pressure.

V. ACKNOWLEDGMENTS

AFG acknowledges support of IPGP during his stay in Paris. AFG also acknowledges support of the National Science Foundation (EAR-1128867, EAR 1520648; EAR 1531583). Experimental development has been possible thanks to the Cellule Projet at IMPMC laboratory.

* agoncharov@carnegiescience.edu
† michel.gauthier@upmc.fr

[1] J. Van Kranendonk, "Solid hydrogen, theory of the properties of solid H_2, HD, and D_2," (Springer US, 1983).
[2] I. F. Silvera, Reviews of Modern Physics **52**, 393 (1980).
[3] J. M. McMahon, M. A. Morales, C. Pierleoni, and D. M. Ceperley, Reviews of Modern Physics **84**, 1607 (2012).
[4] H.-K. Mao and R. J. Hemley, Reviews of Modern Physics **66**, 671 (1994).
[5] A. F. Goncharov, R. J. Hemley, and H.-K. Mao, The Journal of Chemical Physics **134**, 174501 (2011).
[6] I. F. Silvera and R. J. Wijngaarden, Physical Review Letters **47**, 39 (1981).
[7] A. F. Goncharov, I. Mazin, J. H. Eggert, R. J. Hemley, and H.-K. Mao, Physical Review Letters **75**, 2514 (1995).
[8] I. Mazin, R. J. Hemley, A. F. Goncharov, M. Hanfland, and H.-K. Mao, Physical Review Letters **78**, 1066 (1997).
[9] M. Eremets and I. Troyan, Nature Materials **10**, 927 (2011).
[10] R. T. Howie, C. L. Guillaume, T. Scheler, A. F. Goncharov, and E. Gregoryanz, Physical Review Letters **108**, 125501 (2012).
[11] C. J. Pickard and R. J. Needs, Nature Physics **3**, 473 (2007).
[12] P. Dalladay-Simpson, R. T. Howie, and E. Gregoryanz, Nature **529**, 63 (2016).
[13] M. Eremets, I. Troyan, and A. Drozdov, arXiv preprint arXiv:1601.04479 (2016).
[14] A. F. Goncharov, S. T. John, H. Wang, J. Yang, V. V. Struzhkin, R. T. Howie, and E. Gregoryanz, Physical Re-

view B **87**, 024101 (2013).
[15] R. T. Howie, I. B. Magdău, A. F. Goncharov, G. J. Ackland, and E. Gregoryanz, Physical Review Letters **113**, 175501 (2014).
[16] B. Monserrat, R. J. Needs, E. Gregoryanz, and C. J. Pickard, Physical Review B **94**, 134101 (2016).
[17] A. F. Goncharov and J. Crowhurst, Phase Transitions **80**, 1051 (2007).
[18] D. Kirzhnits, Zhur. Eksptl'i Teoret. Fiz. **38** (1960).
[19] A. Abrikosov, Soviet Physics JETP-USSR **12**, 1254 (1961).
[20] E. Babaev, A. Sudbø, and N. Ashcroft, Physical Review Letters **95**, 105301 (2005).
[21] E. Pollock, T. A. Bruce, G. Chester, and J. Krumhansl, Physical Review B **5**, 4180 (1972).
[22] S. M. Stishov, Philosophical Magazine B **81**, 179 (2001).
[23] P. Loubeyre, R. LeToullec, D. Hausermann, M. Hanfland, R. J. Hemley, H.-K. Mao, and L. Finger, Nature **383**, 702 (1996).
[24] G. N. Greaves, A. Greer, R. Lakes, and T. Rouxel, Nature Materials **10**, 823 (2011).
[25] P. Mott and C. Roland, Physical Review B **80**, 132104 (2009).
[26] J. Romain, A. Migault, and J. Jacquesson, Journal of Physics and Chemistry of Solids **37**, 1159 (1976).
[27] C.-S. Zha, H.-K. Mao, and R. J. Hemley, Proceedings of the National Academy of Sciences **97**, 13494 (2000).
[28] C.-S. Zha, H.-K. Mao, and R. J. Hemley, Physical Review B **70**, 174107 (2004).
[29] C.-S. Zha, T. S. Duffy, H.-K. Mao, and R. J. Hemley, Physical Review B **48**, 9246 (1993).
[30] A. Grechnev, S. Tretyak, Y. A. Freiman, A. F. Goncharov, and E. Gregoryanz, Physical Review B **92**, 024102 (2015).
[31] Y. A. Freiman, A. Grechnev, S. Tretyak, A. F. Goncharov, and E. Gregoryanz, Low Temperature Physics **41**, 445 (2015).
[32] E. Brody, H. Shimizu, H.-K. Mao, P. Bell, and W. A. Bassett, Journal of Applied Physics **52**, 3583 (1981).
[33] H. Shimizu, E. Brody, H.-K. Mao, and P. Bell, Physical Review Letters **47**, 128 (1981).
[34] S. Ayrinhac, M. Gauthier, L. E. Bove, M. Morand, G. Le Marchand, F. Bergame, J. Philippe, and F. Decremps, The Journal of Chemical Physics **140**, 244201 (2014).
[35] F. Decremps, D. Antonangeli, M. Gauthier, S. Ayrinhac, M. Morand, G. L. Marchand, F. Bergame, and J. Philippe, Geophysical Research Letters **41**, 1459 (2014).
[36] F. Decremps, M. Gauthier, S. Ayrinhac, L. Bove, L. Belliard, B. Perrin, M. Morand, G. Le Marchand, F. Bergame, and J. Philippe, Ultrasonics **56**, 129 (2015).
[37] E. Peronne and B. Perrin, "Ultrafast acoustics, ultrasonics 56, 2015," (Elsevier, Amsterdam, NL, 2015).
[38] B. Perrin, C. Rossignol, B. Bonello, and J.-C. Jeannet, Physica B: Condensed Matter **263**, 571 (1999).
[39] S. M. Nikitin, N. Chigarev, V. Tournat, A. Bulou, D. Gasteau, B. Castagnede, A. Zerr, and V. E. Gusev, Scientific Reports **5** (2015).
[40] G. Pratesi, L. Ulivi, F. Barocchi, P. Loubeyre, and R. Le Toullec, Journal of Physics: Condensed Matter **9**, 10059 (1997).
[41] A. Dewaele, J. Eggert, P. Loubeyre, and R. Le Toullec, Physical Review B **67**, 094112 (2003).
[42] G. Steinle-Neumann, L. Stixrude, and R. E. Cohen, Physical Review B **60**, 791 (1999).
[43] Y. A. Freiman, S. Tretyak, A. F. Goncharov, H.-K. Mao, and R. J. Hemley, Low Temperature Physics **37**, 1038 (2011).
[44] Y. A. Freiman, A. Grechnev, S. Tretyak, A. F. Goncharov, and R. J. Hemley, Physical Review B **86**, 014111 (2012).
[45] Y. A. Freiman, A. Grechnev, S. Tretyak, A. F. Goncharov, and R. J. Hemley, Low Temperature Physics **39**, 423 (2013).
[46] Y. A. Freiman, S. Tretyak, A. Grechnev, A. F. Goncharov, and R. J. Hemley, Physical Review B **90**, 024501 (2014).
[47] M. Born and K. Huang, "Dynamical theory of crystal lattices," (Oxford University Press, London, UK, 1954).
[48] M. A. Carpenter and E. K. H. Salje, European Journal of Mineralogy **10**, 693 (1998).
[49] R. Hemley, H.-K. Mao, L. Finger, A. Jephcoat, R. Hazen, and C. Zha, Physical Review B **42**, 6458 (1990).